Chemical Methodologies 8(2024) 164-176

Chemical Methodologies

Journal homepage: http://chemmethod.com

Original Article

Green Synthesis of Ag-Se doped ZnO-Co_3O_4-NiO Fivenary Nanocomposite using Poly Anionic Cellulose and Evaluation of Their Anticancer and Photocatalyst Applications

Zahra Sabouri[1], Shirin Sammak[1], Sajjad Sabouri[2], Samaneh Sadat Tabrizi Hafez Moghaddas[1], Majid Darroudi[3,*]

[1]*Department of Medical Biotechnology and Nanotechnology, Faculty of Medicine, Mashhad University of Medical Sciences, Mashhad, Iran*
[2]*Natural Disasters Prevention Research Center, School of Civil Engineering, Iran University of Science and Technology, Tehran, Iran*
[3]*Department of Basic Medical Sciences, Neyshabur University of Medical Sciences, Neyshabur, Iran*

ARTICLEINFO

Article history
Submitted: 2024-01-18
Revised: 2024-01-31
Accepted: 2024-02-10
Manuscript ID: CHEMM-2401-1758
Checked for Plagiarism: Yes
Language check: Yes

DOI:10.48309/CHEMM.2024.436507.1758

KEYWORDS
Ag-Se doped ZnO-Co_3O_4-NiO fivenary Nanocomposite
Poly anionic cellulose
Photocatalytic
Anticancer

ABSTRACT

This study was conducted to evaluate the photocatalytic applications and the cytotoxicity effects of Ag-Se doped ZnO-Co_3O_4-NiO fivenary nanocomposite synthesized using polyanionic cellulose (PAC) polymer as a stabilizer agent. Several procedures such as XRD, FESEM, FTIR, EDX, PSA, and UV-Vis were applied to investigate synthesized nanocomposite. Consistent with the FTIR spectrum, chemical bonds were seen in the structure of the nanocomposite which approved the successful synthesis of them. The XRD pattern of the synthesized nanocomposite revealed sharp diffraction peaks with high crystallinity, and pure phases of Se, Ag, ZnO, NiO, and Co_3O_4 were approved with XRD analysis. FESEM/PSA images indicate that nanocomposite was synthesized with an average size of 23-49 nm and relatively uniformly distributed, in addition, it has a spherical morphology. The synthesized nanocomposite exhibited excellent photocatalytic activity to methyl orange (MO) dye degradation under a UVA light source. The degradation rate of nanocomposite reached 99% within 80 min. The kinetic studies indicate that the degradation of MO dye follows a first-order kinetic model. The cytotoxicity of the nanomaterial was assessed on normal mouse fibroblast NIH3T3 and cancer mouse melanoma B16F0 cell lines with the MTT assay. The results of the MTT test revealed significant cytotoxic influences on cancer B16F0 cells (IC_{50} value = 258.5 µg/mL) in comparison to normal cells.

* Corresponding author: Majid Darroudi
E-mail: darroudim@mums.ac.ir, majiddarroudi@gmail.com

GRAPHICAL ABSTRACT

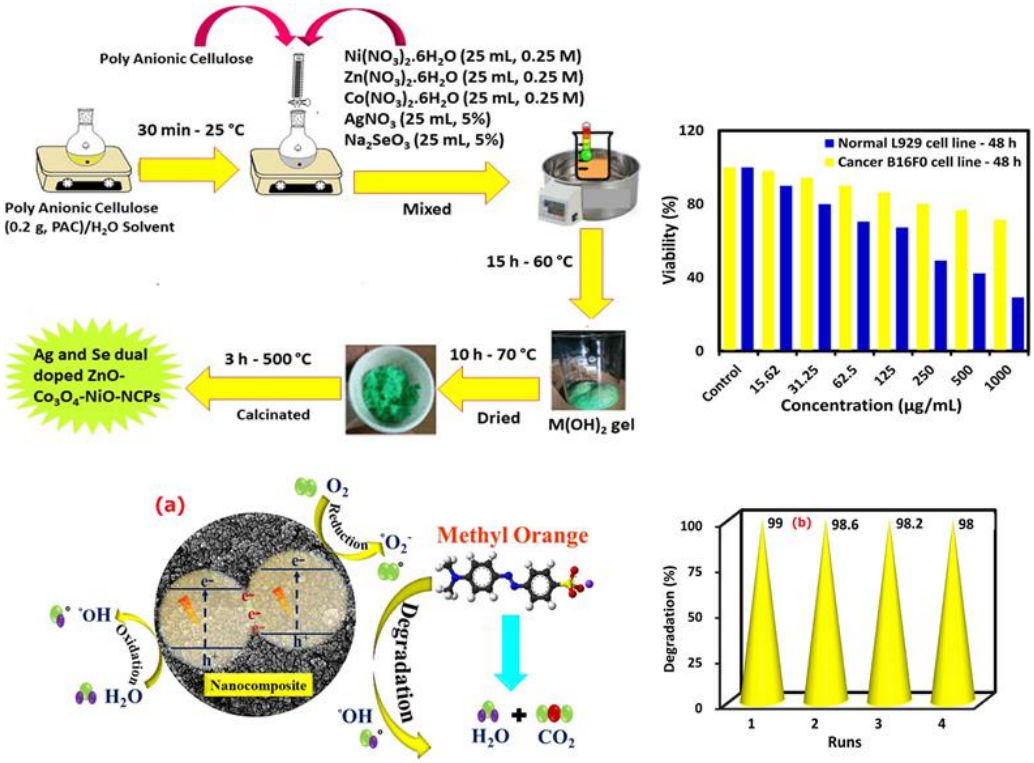

Introduction

Industrial effluents and wastewater generated from organic dye usage are typically toxic to aquatic organisms and humans [1]. Therefore, the efficient and environmentally friendly removal of dyes from wastewater is of utmost importance for clean production practices. Conventional treatment methods for organic dye wastewater are expensive, time-consuming, prone to secondary pollution, and often result in incomplete degradation [2]. In this regard, photocatalytic technology offers a promising solution for the more effective degradation of dye wastewater. Among the various photocatalysts, metal oxides have garnered attention due to their desirable properties such as non-toxicity, chemical inertness, and durability [3-5]. To enhance the photocatalytic activity of metal oxides, several methods have been extensively investigated, including compounding, noble metal deposition, and doping with metal and non-metal ions. Metal oxides (MOs) play an important role in various fields of science, such as chemistry, physics, medicine, and engineering [6,7]. MOs with nanostructured morphologies are widely studied due to their remarkable optical [8], chemical [9], and photocatalytic properties [10-12]. It is also known that these properties depend on both the morphology and the size of the nanoparticles. However, the processes for controlling particle morphology and size are often complex and expensive [13]. Morphological diversity is one of the remarkable features of NCPs which formed 0 to 3D nanoparticles [14], nanowires [15], nanofibers [16], nanorods [17,18], and nanosheets [19]. It was found that 1-D structures are excellent for gas sensing applications due to their high surface-to-volume ratio [20], while 2-D structures, along with gas sensing devices, are more suitable for constructing supercapacitors and other devices [21]. Although pure nanocomposites have numerous applications, doping them with different metals can improve their properties and make them suitable for many other potential applications [22]. As is well-known, doping is the process of introducing impurities into a semiconductor to modify its conductivity or properties. It was found that doping of

nanocomposite can be performed with different elements such as Se and Ag. Se is a practical method for modifying its optical properties and Silver (Ag) is another metal that could be used for doping nanocomposite due to its high solubility and large ion size [22]. In addition, Ag and Se ions can act as acceptors when doped with ZnO-Co_3O_4-NiO nanocomposite due to their excellent properties and potential for easy substitution.

In this study, an eco-friendly route was presented for the synthesis of Ag/Se doped ZnO-Co_3O_4-NiO fivenary nanocomposite using PAC polymer as a stabilizing agent [23]. This method has some advantages including simplicity, environmental compatibility, low-cost, high-purity precursors, and the production of minimal by-products. Moreover, the Ag/Se doped ZnO-Co_3O_4-NiO fivenary nanocomposite can be prepared at low temperatures without the use of harmful chemicals [24]. Although research has been conducted on the synthesis method and photocatalytic effect of nanocomposites, there is no report on the use of PAC polymer as a reducing agent for the synthesis of nanocomposite [7].

After synthesis, the Ag-Se doped ZnO-Co_3O_4-NiO fivenary nanocomposite was characterized with FT-IR, FESEM, XRD, PSA, EDX, and UV-Vis analysis. In continuation, the nanocomposite cytotoxicity was evaluated on normal mouse fibroblast NIH3T3 and cancer mouse melanoma B16F0 cell lines usage of the MTT assay. In addition, the synthesized nanocomposite was used as a photocatalyst in methyl orange (MO) degradation under UVA irradiation. So far, no other study has been done on the biosynthesis of Ag/Se doped ZnO-Co_3O_4-NiO fivenary nanocomposite via PAC polymer, which can express the innovation and originality of this study.

Experimental

Reagents

Polyanionic cellulose (PAC), Sodium hydroxide (NaOH, 98%, Merck), $Ni(NO_3)_2.6H_2O$, $Zn(NO_3)_2.6H_2O$, $Co(NO_3)_2.6H_2O$, Na_2SeO_3, $AgNO_3$ (≥ 99%), and methyl orange ($C_{14}H_{14}N_3NaO_3S$) were bought from Sigma or Merck companies. All chemicals were used without further purification. The normal mouse fibroblast NIH3T3 and cancer mouse melanoma B16F0 lines were prepared of the Pasteur Institute, Iran.

Preparation of Ag/Se Doped Zno-Co_3O_4-Nio Fivenary Nanocomposite

In this study, the Ag/Se doped ZnO-Co_3O_4-NiO fivenary nanocomposite was synthesized using the eco-friendly method. Initial, solutions of $Ni(NO_3)_2.6H_2O$ (25 mL, 0.25 M), $Zn(NO_3)_2.6H_2O$ (25 mL, 0.25 M), and $Co(NO_3)_2.6H_2O$ (25 mL, 0.25 M) salts were prepared separately, and then the solution of the salts was mixed and stirred at room temperature for 15 min (A). Afterwards, the prepared solutions of $AgNO_3$ (25 mL, 5%) and Na_2SeO_3 (25 mL, 5%) were added to A solution and stirred for another 15 min (B). Thereafter, 0.2 g of polyanionic cellulose (PAC) polymer was dissolved in deionized water to obtain the PAC solution (C). Next, 30 mL C solution was added to the B solution and the resulting mixture was stirred at 60 °C for 15 h. The collected gel was placed in the oven at 70 °C (10 h) and then calcinated at 500 °C (3 h) to achieve Ag/Se doped ZnO-Co_3O_4-NiO fivenary nanocomposite [25,26]. The preparation plan of the nanomaterial is exhibited in Figure 1.

Characterization

The characterization of Ag/Se doped ZnO-Co_3O_4-NiO fivenary nanocomposite was done with numerous studies. The chemical bonds presence in the synthesized sample was approved via FTIR analysis. The optical properties of nanomaterials were examined using UV-Vis analysis. FESEM/EDX device was employed to assess the morphology of the synthesized nanomaterial. The determination of the phase and crystal structure of nanomaterial was assessed using the XRD pattern.

Statistical Analysis

The Prism® software and ANOVA test were used for the investigation results of the MTT studies. The p-value ≤ 0.05 was considered significant. Also, Image J® software and IBM SPSS 22® software were applied to the dragging of particle size distribution curves

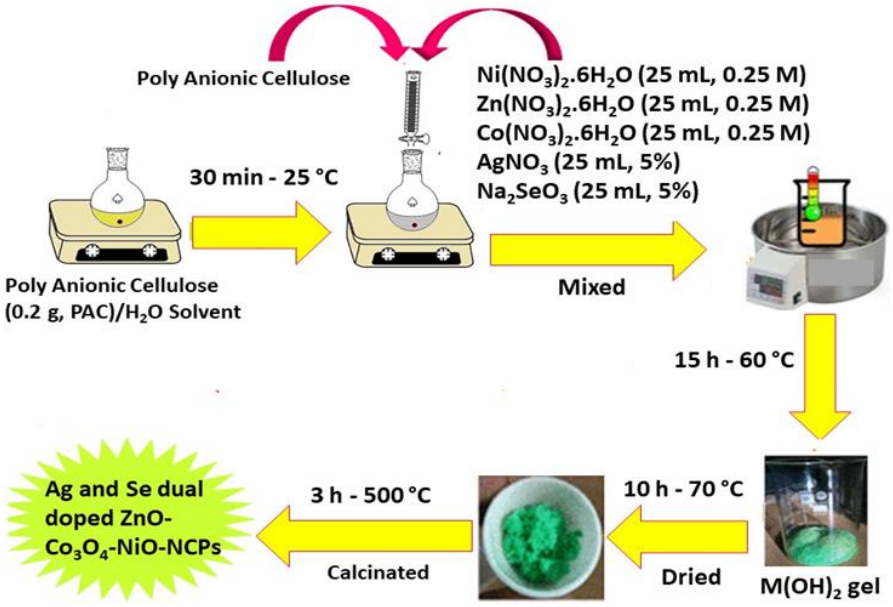

Figure1: Synthesis plan of the nanocomposite

Cell Section

Culture of Cell

After DMEM media preparation with FBS (10%)/antibiotic (1%), normal NIH3T3 and cancer B16F0 cell lines were posited for 24 h on the 96-well plate to stick to the bottom of the well under incubation conditions of 37 °C and 5% CO_2.

Cytotoxicity

The cytotoxicity of Ag/Se doped ZnO-Co_3O_4-NiO fivenary nanocomposite was assessed on the normal mouse fibroblast NIH_3T_3 and cancer mouse melanoma B16F0 cell lines through MTT assay [27,28]. Cells were initally posited on the 96-well plate (7×10^3 cells in each well) to stick to the bottom of each well under incubation conditions of 37 °C and 5% CO_2 for 24 h. Next, the cells were treated with several concentrations of nanomaterial (0 and 1000 µg/mL) for 48 h. In the continuing, the MTT solution (50 uL, 5.0 mg/mL) was added to every well and incubated for 4 h. Afterwards, 100 µL of dimethyl sulfoxide (DMSO) was appended to each well and shaken for 15 min to dissolve formazan crystals. In the final, the absorbance was measured at 630 nm and the cell survival was calculated usage of Equation (1). The cytotoxicity tests were performed in triplicate.

$$Cell\ survival\ (\%) = \frac{A_t}{A_C} \times 100 \qquad (1)$$

Where A_t indicates the treated sample and A_c denotes the control group. The outcomes of the MTT assay (Figure 2) showed dose-dependent toxicity of nanocomposite on cancer B16F0 cells contrasted to normal NIH3T3 cells. The IC_{50} value showed that nanocomposite can inhibit cancer cells after 48 h in a concentration of 258.5 µg/mL. Also, outcomes revealed that synthesized nanomaterials can prevent the growth of cancer cells in a dose-dependent behavior, but no inhibition effects were observed on normal NIH_3T_3 cells.

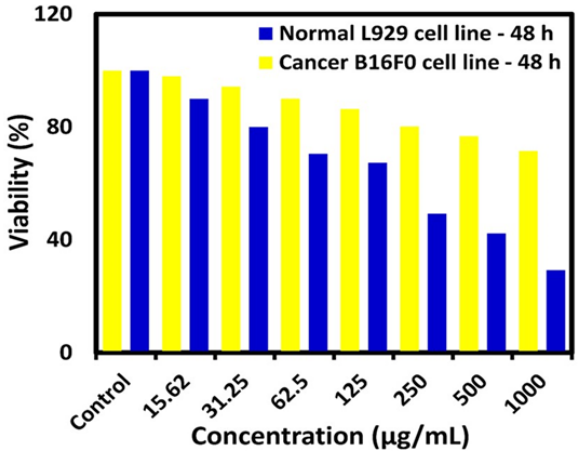

Figure 2: Result of the MTT assay on mouse fibroblast NIH3T3 and mouse melanoma B16F0 cell lines after 48 h, *P*-value <0.05 is considered significant (n = 3)

Photocatalytic Application

Assessment of Photodegradation

According to the details designated elsewhere, an MO photodegradation test was conducted [29,30]. The photocatalytic degradation of the nanocomposite was examined for 80 min, and the outcomes are presented in Figure 3a.

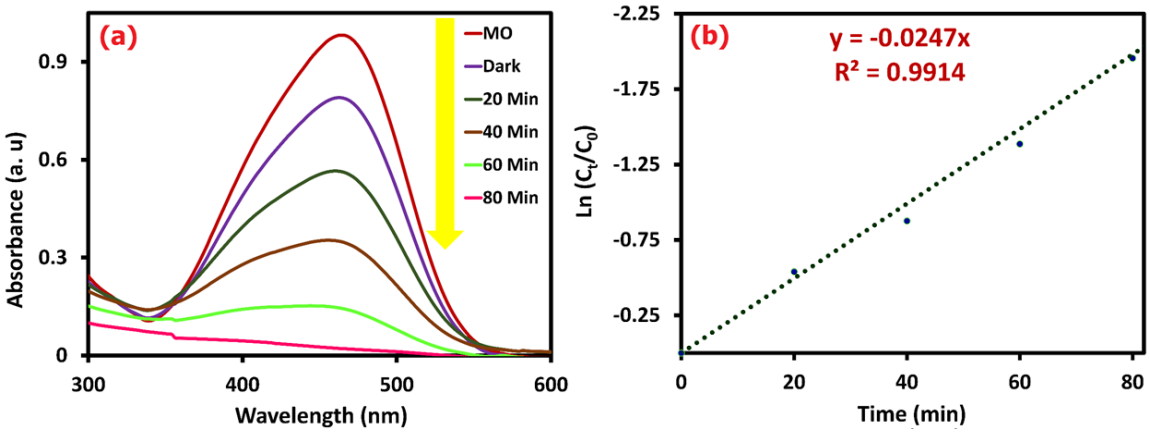

Figure 3: UV-Vis results for photocatalytic test (a) and kinetic chart for MO photodegradation (b)

The photocatalytic degradation test was carried out using a hand-made photocatalytic reaction device to investigate the photocatalytic activity of nanocomposite to the degradation of MO pollutant under UV light (20 W, 365 nm) irradiation. The synthesized photocatalyst was added to 50 mL of MO solution with a concentration of 10 mg/L (pH = 9). A blank control was also prepared using the same concentration and volume of MO but without the photocatalyst. The photocatalyst and the MO solution were mixed well, and then the mixture was placed in a dark treatment for 40 min to establish an adsorption equilibrium between the photocatalyst and MO solution. Afterwards, the UV light source was turned on, and the 2 mL suspension of the mixture was centrifuged every 20 min. The absorbance was measured employing a UV-Vis device at the wavelength of 464 nm. The degradation percentage of the MO was computed with Equation 2, which was offered about 99% after 80 min.

$$\text{Degradation (\%)} = \frac{A_0 - A_t}{A_0} \times 100 \qquad (2)$$

Where, A_t indicates time t sample and A_c denotes the pre-radiation sample. It was observed that nanocomposite exhibited significant photocatalytic degradation performance. These findings highlight the high photocatalytic activity of nanocomposite, indicating the useful effect of Ag and Se doping in easing the degradation of MO dye. Based on previous reports, the degradation process of MO dye by the photocatalyst follows the primary reaction kinetic model (Equation 3).

$$\mathrm{Ln}\left(\frac{C_t}{C_0}\right) = K_{obs}t \qquad (3)$$

Where, C_0 point is the initial concentration of MO dye, C_t is the residual concentration of MO (mg/L) after t min of UV irradiation, and k is the reaction rate constant (min^{-1}). The catalyst's activity can be investigated based on the amount of rate constant (K_{obs}). The findings (Figure 3b) showed that the nanocomposite follows the first-order kinetic model with a K_{obs} value equal to 0.0247 min^{-1}.

According to the mechanism of photocatalytic activity (Figure 4 (a)), it is known that with UV light irradiation to the catalyst surface, a large number of superoxide and hydroxyl radicals ($^{\circ}O_2^-$ and OH°) will be generated due to the catalytic effect of the nanocomposite. The $^{\circ}O_2^-$ and OH° radicals have strong oxidizing properties, so they will react with MO dye to oxidize it to decompose into CO_2, H_2O, etc. The hydroxyl radicals and superoxide radicals will continue to degrade, until turning the MO dye into non-harmful ingredient combinations. The reactions of MO dye photodegradation are exhibited below (Reactions 1 to 5).

$$h\nu\ (UV) + \text{Nanocomposite} \rightarrow \text{Nanocomposite}^* + h^+ + e^- \qquad (1)$$

$$H_2O + h^+ \rightarrow H^+ + OH^{\circ} \qquad (2)$$

$$O_2 + e^- \rightarrow O_2^{\circ -} \qquad (3)$$

$$MO + OH^{\circ} \rightarrow \text{Oxidation} \qquad (4)$$

$$MO + O_2^{\circ -} \rightarrow \text{Reduction} \qquad (5)$$

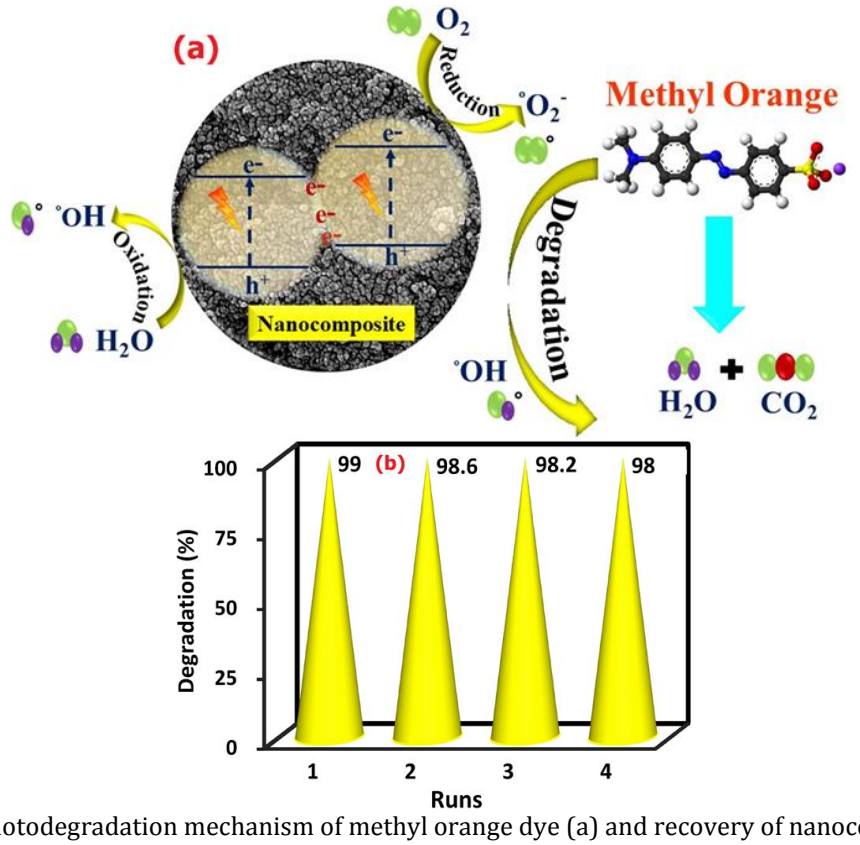

Figure 4: Photodegradation mechanism of methyl orange dye (a) and recovery of nanocomposite (b)

Moreover, the reusability of a catalyst plays an important role in its experimental applications. After a thorough examination of their photocatalytic performance, the Ag/Se doped ZnO-Co_3O_4-NiO fivenary nanocomposite underwent separation via centrifugation (10 min, 10,000 rpm), followed by a washing process involving distilled water and ultimately, drying at 70 °C for 12 h. As evidenced by Figure 4(b), the resultant nanocatalyst was utilized on multiple occasions, with a slight reduction in degradation percentage observed due to the solubility of nanocomposite in the water solvent [35,36].

Results and Discussion

XRD

As demonstrated in Figure 5, the XRD pattern of the Ag/Se doped ZnO-Co_3O_4-NiO fivenary nanocomposite confirmed pure phases of Se, Ag, ZnO, NiO, and Co_3O_4 with crystallite structures. The XRD pattern reveals sharp diffraction peaks, indicating the high crystallinity of the sample. No additional peaks were observed in the calcined sample, which indicates the high purity of the product. The detected patterns match well with the standard card #JCPDS#36-145, approving the hexagonal structure of ZnO. These diffraction peaks appear at 2θ of 31.96, 34.65, 36.44, 47.70, 56.73, 63.09, 66.53, 68.26, and 69.39°, which matching the crystallographic planes of (100), (002), (101), (102), (110), (103), (200), (112), and (201), respectively [31,32]. The XRD peaks, detected at 2θ: 36.93, 42.82, 62.6, 75.3, and 79.2°, were related via (111), (200), (220), (311), and (222) crystal planes that cubic crystalline structure (FCC) of NiO. The XRD peaks detected at 2θ: 19.3°, 31.2°, 36.8°, 44.8°, 59.3°, and 65.2° are correlated to the (111), (220), (311), (400), (511), and (440) crystal planes which confirmed face-centered cubic (FCC) structure of Co_3O_4.

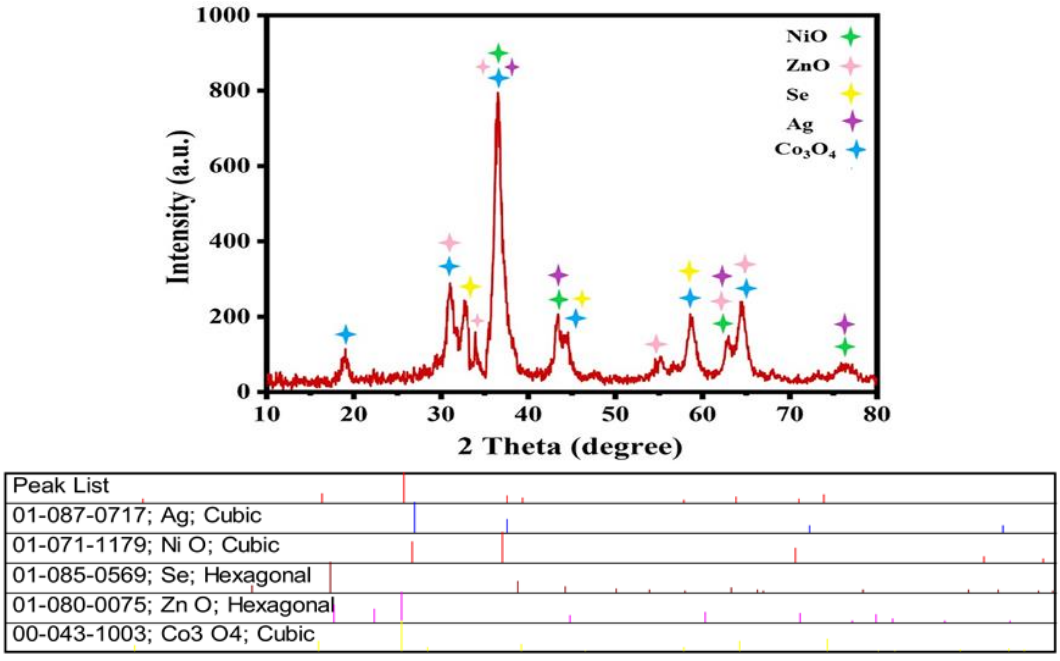

Figure 5: XRD of the nanocomposite

The XRD peaks revealed the cubic structure of Ag at 2θ: 38.25°, 44.41°, 64.55°, and 77.60° which are in accordance via (111), (200), (220), and (311) planes [33,34]. The peaks observed at 2θ: 23.02°, 31.49°, 44.40°, 45.80°, and 56.0° correspond to (100), (101), (012), and (110) planes that are indicative of the hexagonal structure of Se [35,36]. The size of the nanocomposite was computed through Equation 4, which was about 33 nm.

$$D\ (nm) = \frac{k\lambda}{\beta\ cos\ \theta} \quad (4)$$

Where,
D = Particle size (nm)
λ = 0.154 nm and β represents the FWHM (rad)
θ = Angle (degree).

FTIR

To examine the chemical structure and type of bonds, the FT-IR spectrum of Ag/Se doped ZnO-Co_3O_4-NiO fivenary nanocomposite was presented in the range of 400 to 4000 cm^{-1} (Figure 6(a)). According to the comparison table of functional groups in the infrared spectrum, the range of 3351 to 3528 cm^{-1} shows wide absorption peaks, which may be owing to the free and bonded hydroxyl groups. The O-H stretching vibrations of the H_2O molecules were seen as a strong band at 3426 cm^{-1}. The observed band at 2354 cm^{-1} is due to CO_2 molecules in the air. The strong absorption peak exists at 1621 cm^{-1}, which may be the characteristic peak of O-H bending vibrations of the water molecules. Furthermore, the bands that were seen in the range 400 and 1000 cm^{-1} can be attributed to the stretching vibrations of the metal-oxygen (M-O) bonds. Therefore, based on the infrared absorption spectrum, it is found that nanocomposite was successfully synthesized [25,26].

UV-Vis/Bandgap

UV-Vis spectra of Ag/Se doped ZnO-Co_3O_4-NiO fivenary nanocomposite are presented in Figure 6(b). The absorption band that appeared at the wavelength of 316 nm is attributed to ligand-to-metal charge transfers (LMCT). The absorption bands in UV areas could also be owing to the electron move of the valence band to the conduction band. As a consequence, electron-hole recombination reduces, and oxidizing radical creation rises which leads to increasing photoreaction performance. Using the data of the UV-Vis spectrum, the graph of $(\alpha h\nu)$ in terms of $h\nu$ drawn, and the band gap energy was obtained from the point of intersection of the tangent line on the curve with the horizontal axis.

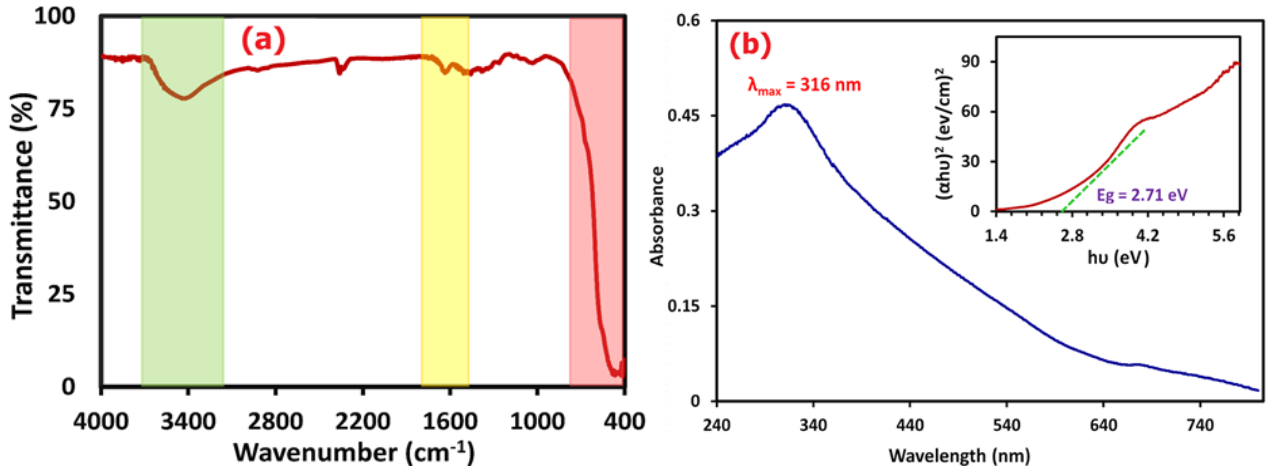

Figure 6: FTIR analysis (a) and UV-Vis/Bandgap spectra (b) of the nanocomposite

Equation (5) was used to obtain the band gap energy of the nanocomposite. The band gap diagram of the nanocomposite is presented in Figure 6(b). The amount of band gap energy calculated was equal to 2.71 eV [37,38].

$$(\alpha h\nu)^n = A\left(h\nu - E_g\right) \quad (5)$$

Where,
$h\nu$ (eV) = Photon energy
α = Absorbance coefficient
A = Constant and $n = 2$ for direct transmittances and $n = 0.5$ for indirect transmittances.

FESEM/EDX/PSA

The morphology, size, and elements distribution of Ag/Se doped ZnO-Co_3O_4-NiO fivenary nanocomposite was investigated through FESEM/EDX/PSA images and the results are presented in Figure 7(a-g).

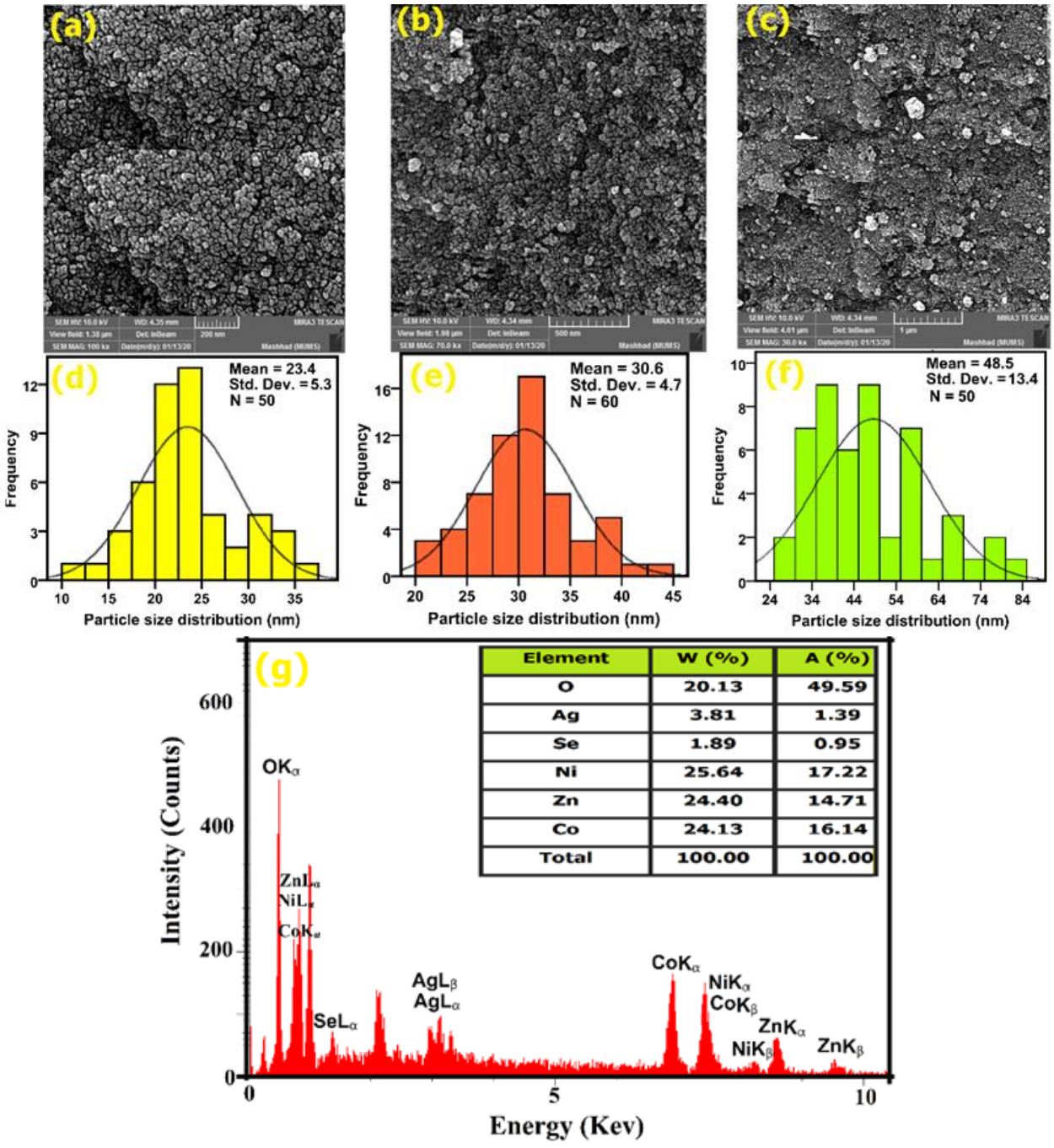

Figure 7: FESEM images (a–c), PSA curves (d–f), and EDX analysis (g) of the nanocomposite

The results show that the nanocomposite was synthesized with high purity. FESEM images (Figure 7(a-c)), indicate that nanocomposite was synthesized with small particle size, relatively uniformly distributed, and completely developed crystals, and also has a spherical morphology. The size average of the nanocomposite was found to be about 23 to 48.5 nm using the PSA curves (Figure 7(d-f)). The particle size distribution is consistent with the obtained results of the XRD pattern. To know the quantity and nature of the elements used, as well as the amount of element

dispersion in the synthesized sample, the nanocomposite was analyzed by the EDX technique. As shown in Figure 7(g), clear six elements of O, Se, Ag, Ni, Co, and Zn were detected in the synthesized sample, and the weight and atomic percentages of the elements were inserted in Figure 7(g) [39,40].

Conclusion

In this study, Ag/Se doped ZnO-Co_3O_4-NiO fivenary nanocomposite was prepared via polyanionic cellulose (PAC) polymer with the green chemistry method. Different analyses showed that the synthesized nanocomposite has good uniformity and dispersion. The FESEM images showed that these particles have a spherical morphology with uniformity distribution. The cytotoxicity of the nanocomposite was assessed on NIH3T3 and B16F0 cell lines with the MTT test. The results revealed significant cytotoxic influences on cancer B16F0 cells (IC_{50} = 258.5 µg/mL) in comparison to normal NIH3T3 cells. The synthesized nanocomposite exhibited excellent photocatalytic activity to MO dye degradation under a UVA light source and the degradation rate reached 99% within 80 min. The experimental results indicate that the degradation of MO dye follows a first-order kinetic model. This study provides a valuable reference and offers solutions to enhance the practical application of photocatalytic materials for wastewater degradation. Concerning the high efficiency of the photocatalytic process, we recommend utilizing this method for the removal of pollutants in water and wastewater treatment processes.

Funding

This project was financially supported by the Vice-Chancellor for Research (Grant no. 4011401), Mashhad University of Medical Sciences.

Conflict of Interest

The authors declare that they have no conflict of interest in this study.

Ethical Approval

No experiments are conducted on animals or humans.

Availability of Data and Material

Not applicable.

ORCID

Majid Darroudi
https://orcid.org/0000-0002-2624-7242

References

[1]. Emelu, Victoria O., C. Emelu, B.B. Babatunde, E. Wali, O.O. Afolabi, Associated Disaster Risk of Inadequate Corrosion Control (Cathodic Protection) on Pipelines in Port Harcourt, Nigeria: A Quantitative Approach, *Journal of Engineering in Industrial Research*, 2023, **4**:22 [Crossref], [Google Scholar], [Publisher]
[2]. Khalid Hamood Al-Behadili W., Jawad Y.M., Hasan H.J., Study the Effect of PH on Absorption and Fluorescence Spectra of Eosin Y Dye in Ethanol, *Asian Journal of Green Chemistry*, 2023, **7**:163 [Crossref], [Publisher]
[3]. Hakimi M., Kiani P., Alikhani M., Feizi N., Bajestani A.M., Alimard P., Reducing environmental pollution of fuel fly ash by extraction and removal vanadium pentoxide, *Solid Fuel Chemistry*, 2020, **54**:337 [Crossref], [Google Scholar], [Publisher]
[4]. Algheryani K.M., Asweisi A.A., Cloud Point Extraction of Trivalent Chromium from Aqueous Solutions Using Different Nonionic Surfactants, *Journal of Engineering in Industrial Research*, 2023, **4**:68 [Crossref], [Google Scholar], [Publisher]
[5]. Johnson A., Investigating the Effects of Environmental Applications on Decomposition of Zein Nanoparticles in Adsorbents in Industry, *Journal of Engineering in Industrial Research*, 2023, **4**:92 [Crossref], [Publisher]

[6]. Martínez D.S., Martínez-De La Cruz A., Cuéllar E.L., Photocatalytic properties of WO_3 nanoparticles obtained by precipitation in presence of urea as complexing agent, *Applied Catalysis A: General*, 2011, **398**:179 [Crossref], [Google Scholar], [Publisher]
[7]. Ghazal S., Mirzaee M., Darroudi M., Green synthesis of tungsten oxide (WO_3) nanosheets and investigation of their photocatalytic and cytotoxicity effects, *Micro & Nano Letters*, 2022, **17**:286 [Crossref], [Google Scholar], [Publisher]
[8]. Liqiang J., Yichun Q., Baiqi W., Shudan L., Baojiang J., Libin Y., Wei F., Honggang F., Jiazhong S., Review of photoluminescence performance of nano-sized semiconductor materials and its relationships with photocatalytic activity, *Solar Energy Materials And Solar Cells*, 2006, **90**:1773 [Crossref], [Google Scholar], [Publisher]
[9]. Cheng W., Baudrin E., Dunn B., Zink J.I., Synthesis and electrochromic properties of mesoporous tungsten oxideBasis of a presentation given at Materials Discussion No. 3, 26–29 September, 2000, University of Cambridge, UK, *Journal of Materials Chemistry*, 2001, **11**:92 [Crossref], [Google Scholar], [Publisher]
[10]. Chen D., Ye J., Hierarchical WO_3 hollow shells: dendrite, sphere, dumbbell, and their photocatalytic properties, *Advanced Functional Materials*, 2008, **18**:1922 [Crossref], [Google Scholar], [Publisher]
[11]. Hakimi M., Alikhani M., Characterization of α-Fe_2O_3 Nanoparticles Prepared from a New [Fe (Ofloxacin)$_2$Cl$_2$] Precursor: A Heterogeneous Photocatalyst for Removal of Methylene Blue and Ciprofloxacin in Water, *Journal of Inorganic and Organometallic Polymers and Materials*, 2020, **30**:504 [Crossref], [Google Scholar], [Publisher]
[12]. Hassan M.K., Karim M.T., Biswas P., Howlader D., Harun-Ur-Rashid M., Kumer A., Computational Investigation for Tetragonal Crystals of $Zn(GaS_2)_2$, $Zn(GaSe_2)_2$, and $Zn(GaTe_2)_2$ Photocatalysts for Wastewater Treatment: First Principle Approaches, *Advanced Journal of Chemistry-Section B: Natural Products and Medical Chemistry*, 2024, **6**:46 [Crossref], [Publisher]
[13]. Byzynski G., Melo C., Volanti D.P., Ferrer M.M., Gouveia A.F., Ribeiro C., Andrés J. ,Longo E., The interplay between morphology and photocatalytic activity in ZnO and N-doped ZnO crystals, *Materials & Design*, 2017, **120**:363 [Crossref], [Google Scholar], [Publisher]
[14]. Martínez-de La Cruz A., Martínez D.S., Cuéllar E.L., Synthesis and characterization of WO_3 nanoparticles prepared by the precipitation method: evaluation of photocatalytic activity under vis-irradiation, *Solid state sciences*, 2010, **12**:88 [Crossref], [Google Scholar], [Publisher]
[15]. Long H., Zeng W., Zhang H., Synthesis of WO 3 and its gas sensing: A review, *Journal of Materials Science: Materials in Electronics*, 2015, **26**:4698 [Crossref], [Google Scholar], [Publisher]
[16]. Cao S., Zhao C., Han T., Peng L., Hydrothermal synthesis, characterization and gas sensing properties of the WO_3 nanofibers, *Materials Letters*, 2016, **169**:17 [Crossref], [Google Scholar], [Publisher]
[17]. Zhou Y., Yang L., Li S., Dang Y., A novel electrochemical sensor for highly sensitive detection of bisphenol A based on the hydrothermal synthesized Na-doped WO_3 nanorods, *Sensors and Actuators B: Chemical*, 2017, **245**:238 [Crossref], [Google Scholar], [Publisher]
[18]. Ren Y., Xu Q., Zheng X., Fu Y., Wang Z., Chen H., Weng Y., Zhou Y., Building of peculiar heterostructure of Ag/two-dimensional fullerene shell-WO_{3-x} for enhanced photoelectrochemical performance, *Applied Catalysis B: Environmental*, 2018, **231**:381 [Crossref], [Google Scholar], [Publisher]
[19]. Yu Y., Zeng W., Xu M., Peng X., Hydrothermal synthesis of $WO_3 \cdot H_2O$ with different nanostructures from 0D to 3D and their gas sensing properties, *Physica E: Low-dimensional Systems and Nanostructures*, 2016, **79**:127 [Crossref], [Google Scholar], [Publisher]
[20]. Miller D.R., Akbar S.A., Morris P.A., Nanoscale metal oxide-based heterojunctions for gas sensing: A review, *Sensors and Actuators B: Chemical*, 2014, **204**:250 [Crossref], [Google Scholar], [Publisher]
[21]. Peng X., Peng L., Wu C., Xie Y., Two dimensional nanomaterials for flexible supercapacitors, *Chemical Society Reviews*, 2014, **43**:3303 [Crossref], [Google Scholar], [Publisher]

[22]. Ghazal S., Akbari A., Hosseini H.A., Sabouri Z., Forouzanfar F., Khatami M., Darroudi M., Biosynthesis of silver-doped nickel oxide nanoparticles and evaluation of their photocatalytic and cytotoxicity properties, *Applied Physics A*, 2020, **126**:1 [Crossref], [Google Scholar], [Publisher]
[23]. Khan M.M., Kumar S., Ahamad T., Alhazaa A.N., Enhancement of photocatalytic and electrochemical properties of hydrothermally synthesized WO_3 nanoparticles via Ag loading, *Journal of Alloys and Compounds*, 2018, **743**:485 [Crossref], [Google Scholar], [Publisher]
[24]. Jamali M., Tehrani F.S., Effect of synthesis route on the structural and morphological properties of WO_3 nanostructures, *Materials Science in Semiconductor Processing*, 2020, **107**:104829 [Crossref], [Google Scholar], [Publisher]
[25]. Sabouri Z., Sabouri M., Moghaddas S.S.T.H., Mostafapour A., Samarghandian S., Darroudi M., Plant-mediated synthesis of Ag and Se dual-doped ZnO-CaO-CuO nanocomposite using Nymphaea alba L. extract: assessment of their photocatalytic and biological properties, *Biomass Conversion and Biorefinery*, 2023, 1 [Crossref], [Google Scholar], [Publisher]
[26]. Sabouri Z., Oskuee R.K., Sabouri S., Moghaddas S.S.T.H., Samarghandian S., Abdulabbas H.S., Darroudi M., Phytoextract-mediated synthesis of Ag-doped ZnO–MgO–CaO nanocomposite using Ocimum Basilicum L seeds extract as a highly efficient photocatalyst and evaluation of their biological effects, *Ceramics International*, 2023, **49**:20989 [Crossref], [Google Scholar], [Publisher]
[27]. Mostafapour A., Baharara J., Khazaei M., Avan A., Hassanian S.M., The angiotensin-converting enzyme inhibitor Enalapril'increases the anti-proliferative activity of 5-Fluorouracil in Colorectal Cancer cells, *Eurasian Journal of Medicine and Oncology*, 2021, **5**:318 [Crossref], [Google Scholar], [Publisher]
[28]. Sabouri Z., Moghaddas S.S.T.H., Mostafapour A., Darroudi M., Biopolymer-template synthesized CaSO4 nanoparticles and evaluation of their photocatalytic activity and cytotoxicity effects, *Ceramics International*, 2022, **48**:16306 [Crossref], [Google Scholar], [Publisher]
[29]. Sabouri Z., Oskuee R.K., Sabouri S., Moghaddas S.S.T.H., Samarghandian S., Abdulabbas H.S., Darroudi M., Phytoextract-mediated synthesis of Ag-doped ZnO–MgO–CaO nanocomposite using Ocimum Basilicum L seeds extract as a highly efficient photocatalyst and evaluation of their biological effects, *Ceramics International*, 2023, **49**:20989 [Crossref], [Google Scholar], [Publisher]
[30]. Sabouri Z., Sabouri M., Amiri M.S., Khatami M., Darroudi M., Plant-based synthesis of cerium oxide nanoparticles using Rheum turkestanicum extract and evaluation of their cytotoxicity and photocatalytic properties, *Materials Technology*, 2022, **37**:555 [Crossref], [Google Scholar], [Publisher]
[31]. Naseer M., Aslam U., Khalid B., Chen B., Green route to synthesize Zinc Oxide Nanoparticles using leaf extracts of Cassia fistula and Melia azadarach and their antibacterial potential, *Scientific Reports*, 2020, **10**:9055 [Crossref], [Google Scholar], [Publisher]
[32]. Klinbumrung A., Panya R., Pung-Ngama A., Nasomjai P., Saowalakmeka J., Sirirak R., Green synthesis of ZnO nanoparticles by pineapple peel extract from various alkali sources, *Journal of Asian Ceramic Societies*, 2022, **10**:755 [Crossref], [Google Scholar], [Publisher]
[33]. Sallehudin T.A.T., Seman M.N.A., Chik S.M.S.T., Preparation and Characterization Silver Nanoparticle Embedded Polyamide Nanofiltration (NF) Membrane, MATEC Web of Conferences, EDP Sciences, 2018, 02003 [Crossref], [Google Scholar], [Publisher]
[34]. Polani S., Melamed S., Burlaka L., De La Vega F., Zitoun D., Large-scale synthesis of polyhedral Ag nanoparticles for printed electronics, *RSC Advances*, 2017, **7**:54326 [Crossref], [Google Scholar], [Publisher]
[35]. Kokila K., Elavarasan, N., Sujatha V., Diospyros montana leaf extract-mediated synthesis of selenium nanoparticles and their biological applications, *New Journal of Chemistry*, 2017, **41**:7481 [Crossref], [Google Scholar], [Publisher]

[36]. Velayati M., Hassani H., Sabouri Z., Mostafapour A., Darroudi M., Biosynthesis of Se-Nanorods using Gum Arabic (GA) and investigation of their photocatalytic and cytotoxicity effects, *Inorganic Chemistry Communications*, 2021, **128**:108589 [Crossref], [Google Scholar], [Publisher]
[37]. Najjar M., Nasseri M.A., Darroudi M., Allahresani A., Synthesis of dihydropyrimidinone and dihydropyridine derivatives by a GQDs-based magnetically nanocatalyst under solvent-free conditions, *Journal of Environmental Chemical Engineering*, 2022, **10**:108854 [Crossref], [Google Scholar], [Publisher]
[38]. Rahman A., Harunsani M.H., Tan A.L., Ahmad N., Min B.K., Khan M.M., Influence of Mg and Cu dual-doping on phytogenic synthesized ZnO for light induced antibacterial and radical scavenging activities, *Materials Science in Semiconductor Processing*, 2021, **128**:105761 [Crossref], [Google Scholar], [Publisher]
[39]. Marsooli M.A., Rahimi-Nasrabadi M., Fasihi-Ramandi M., Adib K., Eghbali-Arani M., Ahmadi F., Sohouli E., Sobhani nasab A., Mirhosseini S.A., Gangali M.R., Preparation of $Fe_3O_4/SiO_2/TiO_2/CeVO_4$ nanocomposites: investigation of photocatalytic effects on organic pollutants, bacterial environments, and new potential therapeutic candidate against cancer cells, *Frontiers in Pharmacology*, 2020, **11**:192 [Crossref], [Google Scholar], [Publisher]
[40]. Anand K.V., Keerthika S., Vasantharaja R., Kannan M., Preetha S., Selvan S.M., Chaturvedi S., Govindaraju K., Biogenic preparation of ZnO, CaO, and ZnO-CaO nanocomposites and its influence on agro-morphological characteristics of mung bean, *Environmental Science and Pollution Research*, 2022, 1 [Crossref], [Google Scholar], [Publisher]

Use your device to scan and read the article online

HOW TO CITE THIS ARTICLE
Zahra Sabouri, Shirin Sammak, Sajjad Sabouri, Samaneh Sadat Tabrizi Hafez Moghaddas, Majid Darroudi. Green Synthesis of Ag-Se doped ZnO-Co_3O_4-NiO fivenary Nanocomposite using Poly Anionic Cellulose and Evaluation of Their Anticancer and Photocatalyst Applications. *Chem. Methodol.*, 2024, 8(3) 164-176
DOI: https://doi.org/10.48309/CHEMM.2024.436507.1758
URL: https://www.chemmethod.com/article_190325.html